Routledge
Taylor & Francis Group

Journal of Sports Sciences

ISSN: 0264-0414 (Print) 1466-447X (Online) Journal homepage: https://www.tandfonline.com/loi/rjsp20

Modelling of rational variants of the speed-skating technique

A.V. Voronov , E.K. Lavrovsky & V.M. Zatsiorsky

To cite this article: A.V. Voronov , E.K. Lavrovsky & V.M. Zatsiorsky (1995) Modelling of rational variants of the speed-skating technique, Journal of Sports Sciences, 13:2, 153-170, DOI: 10.1080/02640419508732222

To link to this article: https://doi.org/10.1080/02640419508732222

Journal of Sports Sciences, 1995, 13, 153–170

Modelling of rational variants of the speed-skating technique

A.V. VORONOV,[1]* E.K. LAVROVSKY[2] and V.M. ZATSIORSKY[3]

[1]*Computer Simulation Laboratory, All Union Research Institute of Sport, Kazakova str. 18, Moscow 103064,* [2]*University of Moscow, Moscow* and [3]*Biomechanics Laboratory, The Pennsylvania State University, University Park, Pennsylvania 16802-3408, USA*

Accepted 6 June 1994

An 11-segment planar model of a speed skater's body was developed and computerized. The solution of the inverse dynamics problem made it possible to determine the net joint moments, reaction moments and the mechanical energy expenditures. The modelling of different variants of skating on the straight parts of the circuit revealed the most efficient one to be the run without arm swing, with the sideward push-off and without an active swing by the recovery leg.

Keywords: Inverse dynamics problem, mechanical energy expenditures, modelling, speed skating, sport technique.

Introduction

This study is concerned with speed skating. Terminology referring to the phases of the skating action must be defined at the outset:

- *Phase 1 (free skate)*: the phase starting from the instant of the push-off skate lifting from the ice and ending when the swing thigh is vertical.
- *Phase 2 (single support push-off)*: the phase starting from the position when the swing thigh is vertical and ending when the swing foot touches the ice.
- *Phase 3 (double support push)*: the phase starting from the swing foot touching the ice and ending with the lifting of the push-off skate from the ice. In this phase, the push-off leg is extended at the hip, knee and ankle joints.

Previous research

The techniques of speed skating have been investigated by a number of authors. Sokolov (1970) analysed the leading elements of the skating technique. Doctorevitch (1976) studied the phase structure of step and support reactions. Van Ingen Schenau (1981) determined the coefficients of aerodynamic resistance of the skater's body at touch-down and calculated the work done in the extension of the push-off leg. De Boer (1986) and Koning *et al.* (1991a, b) investigated the electrical activity and velocity of leg muscle contraction. At the present time, it is possible to state that, although the speed-skating technique has been well investigated, the most efficient technique has still to be established.

Oxygen consumption reaches 50–60 ml kg^{-1} min^{-1} (Ekblom *et al.*, 1967; Di Prampero *et al.*, 1976) at speed-skating velocities of 9.5–10.5 m s^{-1}. According to Kandow *et al.* (1987), the standard deviation of oxygen consumption can reach 8 ml kg^{-1} min^{-1}. Van Ingen Schenau (1981) noted differences in oxygen consumption between elite skaters (body mass 72 kg) of 3 ml kg^{-1} min^{-1}. In a group of well-trained skaters (body mass 72 kg), differences in oxygen consumption of 8 ml kg^{-1} min^{-1} were noted. It is possible to state that at the same skating velocity, metabolic energy expenditure can vary from 400 to 1000 ml min^{-1}. One reason for the difference in oxygen consumption between skaters is the mechanical efficiency of the technique. The most effective technique in cyclic locomotion is such that a greater speed is achieved with low mechanical energy expenditure and hence less metabolic energy.

* To whom all correspondence should be addressed.

The present study

The present paper is concerned with the mechanical energy expenditure of the skating technique on the straights as influenced by the body weight shift on the support leg in phase 3, air resistance and the swing activity of the free leg. A schematic representation of the modelling procedure is presented in Fig. 1.

The study was undertaken in three consecutive stages. First, we developed a two-dimensional mechanical model of the speed-skating technique. The next stage was based on experiments to determine the aerodynamic forces (these are not described in full in this paper) and on the kinematics data of Doctorevitch (1976). From the known average velocities in the three phases and the positions of the skater's body at the boundaries of the phases, the instantaneous velocities and accelerations were estimated using cubic spline functions. Finally, having determined and analysed the reference variants of the speed-skating technique, the third stage involved the solution of the inverse dynamics problem and the comparison of possible variants of speed-skating technique.

The planar speed-skating model

Mechanical model

An 11-segment planar model of the skater's body was developed, which includes torso–head, thigh, shank, foot–skate, upper arm and lower arm–hand segments. Mass-inertial and anthropomorphic data for these segments are given in Table 1. For simplicity, in calculating the moment of inertia, the torso and head were modelled as one spherical segment. Body segments were assumed to be rigid and the joints to be ideal. Figure 2 presents the general view of the model and also the positive direction of angles and joint moments.

The position of the skater's body is defined by 13 co-ordinates (see Fig. 2):

$$Y^0, Z^0, \alpha, \beta_1, \beta_2, \gamma_1, \gamma_2, \eta_1, \eta_2, \xi_1, \xi_2, \theta_1, \theta_2$$

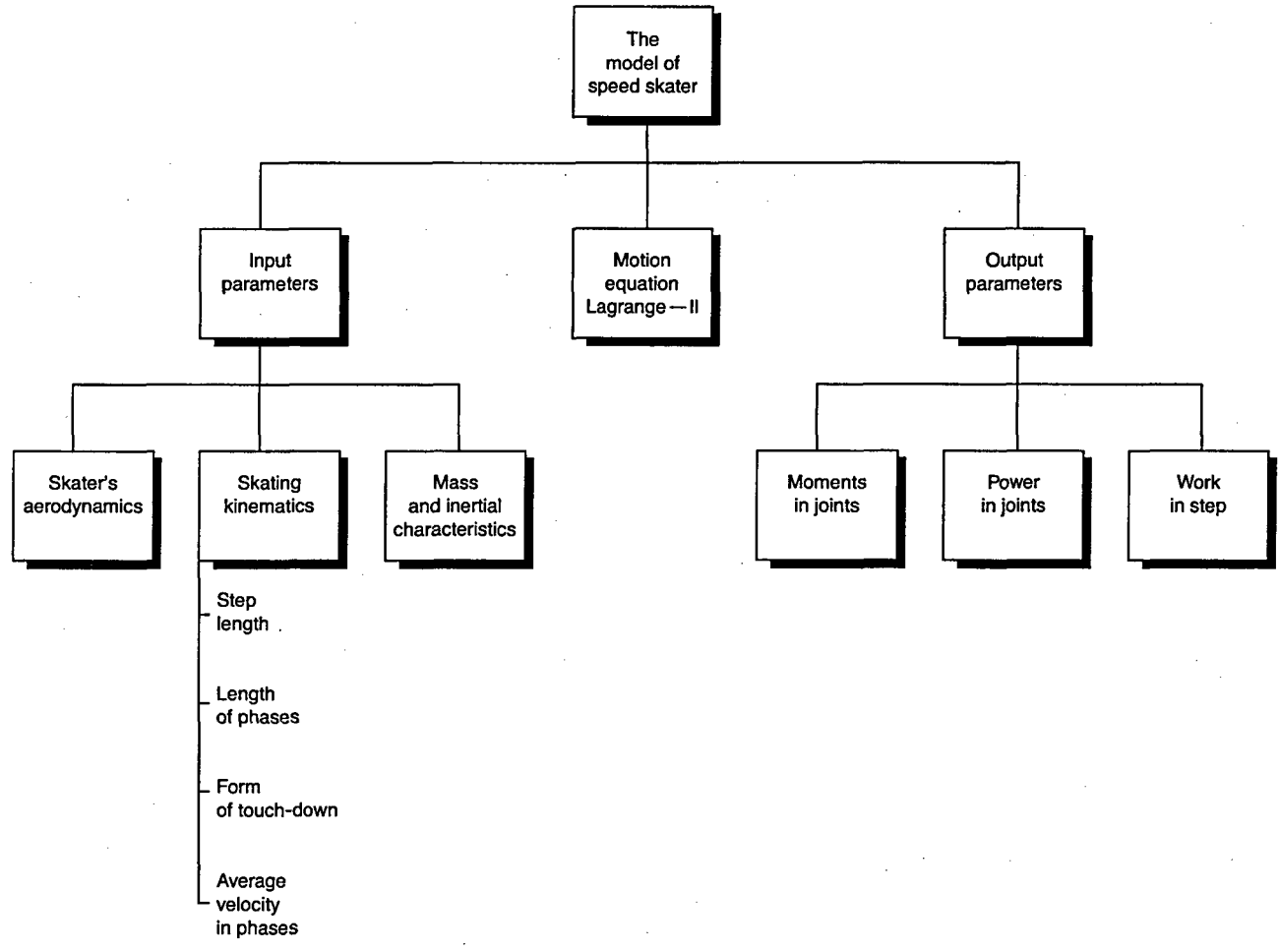

Figure 1 A schematic representation of the speed-skating model.

The equation of motion based on Lagrange-II equations can be written as follows:

$$\frac{d}{dt}\left[\frac{\partial L}{\partial \dot{\lambda}_k}\right]-\frac{\partial L}{\partial \lambda_k}=Q_k \quad (1)$$

where the coordinates λ_k are:

- Y^0, Z^0 = hip-joint co-ordinates (the pole of the model).
- α, β_i, γ_i, η_i, ξ_i, θ_i = the angles to the vertical of corresponding body segments; i = 1, 2, where suffix i = 1 stands for the right leg and i = 2 for the left leg. In all the positions of a speed skater studied, the right leg is the push-off (support) leg and the left leg is the swing-support leg.
- L = the difference between the kinetic and potential energy of the skater's body.
- Q_k = the magnitude of the generalized force.

Using the expression for the kinetic and potential energy of the body segments, and including the data connected with the calculation of derivatives d/dt $[\partial L/\partial \dot{\lambda}_k]$ and $\partial L/\partial \lambda_k$, we obtain the differential equations of the model investigated. It is convenient to present these expressions in a matrix form (Formalsky, 1982):

$$A*\ddot{\lambda}+B*\dot{\lambda}^2+\mathbf{g}\,C*\sin(\lambda)=D*\mathbf{W}+E*\mathbf{R} \quad (2)$$

where 13 * 13 matrices A, B, C, D, E and vectors $\ddot{\lambda}$, $\dot{\lambda}^2$, $\sin(\lambda)$, $\mathbf{W}$, $\mathbf{R}$ are given in Appendix 1; $\mathbf{g}$ is gravitational acceleration.

Vector $\mathbf{R}$ contains the aerodynamic resistance forces of the speed skater's body ($-\mathbf{F}^a$) and the segments ($-\mathbf{F}_j^a$) torso plus head, thigh (left, right), shank including foot and skate (left, right). The aerodynamic drag forces of the arms are omitted. The magnitude of each aerodynamic force ($-F_j^a$) acting on the segments was defined by the equation:

$$F_j^a=S_j*S^{-1}*[0.5*S*\rho*(A_k*v^2+B_k*v+C_k)]*v^2 \quad (3)$$

where ρ is the density of the air (dependent on the temperature and pressure); S_j is the frontal area of the

Table 1 Mass-inertial characteristics of model (body mass 78.7 kg, height 180 cm)

	Segments					
Variable	Torso plus head	Thigh	Shank	Foot plus skate	Upper arm	Lower arm plus hand
Mass (kg)	36.3	13.4	3.46	1.70	1.74	1.73
Moment of inertia (kg m^{-2})	2.59	0.270	0.04	0.0042	0.010	0.0093
Position of segment's mass centre from the proximal joint (m)	0.30	0.16	0.178	0.074	0.10	0.22
Segment length (m)	0.66	0.43	0.40	0.21	0.35	0.38

Note: The position of the torso centre of mass is calculated from the hip joint; the length of the torso is equal to the distance from the hip joint to the shoulder joint. The centre of mass position of the thigh is calculated from the hip joint, that of the shank from the knee joint, and that of the foot from the ankle joint. The centre of mass of the upper arm is calculated from the shoulder joint and the lower arm from the elbow joint.

Mass and inertial characteristics of segments calculated according to Zatsiorsky *et al.* (1981). Moment of inertia about torso of mass calculated according to the formula for an ellipsoid:

$$J_T^0=\frac{m_T}{8(a^2+b^2)}[3(a^4+b^4)+2a^2b^2]$$

where a is approximately 0.395 m and b 0.215 m; mass m_T = 43.3 kg (torso + head + arms).

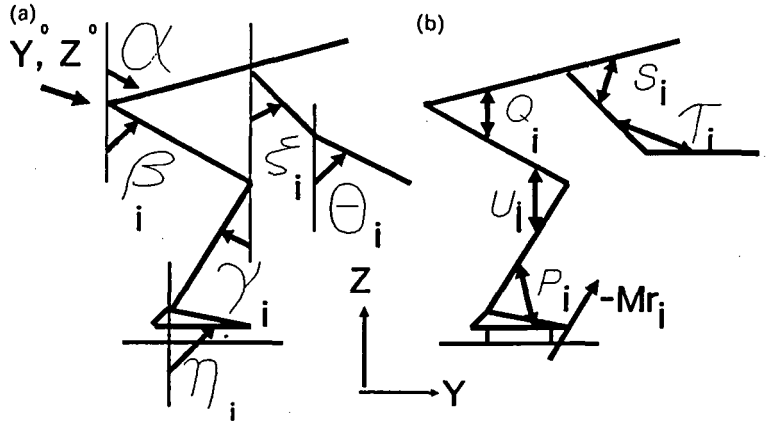

Figure 2 A planar model of the speed skater's body. (a) The positive direction of angular displacement →; (b) the positive direction of the net joint moments ↔.

corresponding segment (j = 1–5); S is the frontal area of the skater's body at touch-down; v is the speed of the centre of mass of the segment (assumed to be equal to the speed of the model pole – the hip joint – plus the opposing wind speed). In the square brackets of equation (3), the aerodynamic force for the whole skater's body ($-F^a$) is presented. The product $S_j * S^{-1}$ is the relative frontal area of the j-th segment. Equation (3) assumes that the aerodynamic forces acting on each segment are proportional to that segment's frontal area.

The terms in parentheses ($A_k * v^2 + B_k * v + C_k$) define the coefficient of the aerodynamic resistance for the speed skater's body, C_x. A_k, B_k, C_k are the coefficients of the regression equation describing the dependence of C_x on the skater's speed. Suffix k stands for the form of touch-down. The coefficients A_k, B_k and C_k depend on the speed and on the selected variant of touch-down. It should be noted that the values S and S_j are dependent on the angles of the joints and on body dimensions. The coefficients A_k, B_k, C_k for calculating C_x and the coefficients of the regressioan equations for calculating each segment's frontal area are given in Tables 4 and 5, respectively, in Appendix 2.

In order to estimate the mechanical energy expenditure of different variants of skating on the straight, the inverse dynamics problem was solved.

The efficiencies of concentric and eccentric mechanical work differ from between 10% and 300% (Zatsiorsky *et al.*, 1986). In the mechanical model investigated, where the muscles at the joints were replaced by the net moments, the physiological efficiencies of 'positive' and 'negative' mechanical work were assumed to be identical. Although this might be considered a limitation of the model, there is, at present, no generally agreed method of estimating metabolic work. The mechanical work W was obtained as the sum of the absolute value of the work done by the net moment for each joint mentioned (Zatsiorsky *et al.*, 1982; Formalsky, 1982; Beletsky, 1984):

$$W = \sum_{l=1}^{5} \sum_{i=1}^{2} \sum_{m=2}^{N} \int_{\phi_i^{l,m-1}}^{\phi_i^{l,m}} |M_i^{l,m}\, d\phi_i^l| \qquad (4)$$

where $M_i^{l,m}$ is the magnitude of the net moment for the l-th joint in the m-th point of the step, and $\phi_i^{l,m}$ is the joint angle. For the hip joint, $\phi_i^{1,m} = \pi - (\alpha^m + \beta_i^m)$; for the knee, $\phi_i^{2,m} = \pi - (\beta_i^m + \gamma_i^m)$; for the ankle joint, $\phi_i^{3,m} = \pi - (\eta_i^m + \gamma_i^m)$; for the shoulder joint, $\phi_i^{4,m} = \pi - (\alpha^m + \xi_i^m)$; for the elbow joint, $\phi_i^{5,m} = \pi - (-\xi_i^m + \theta_i^m)$; where suffix i = 1, 2 stands for the joint (right or left) and m = 2 to N (where N is the number of points in trajectory); $\pi = 3.1416$.

The work output per metre of distance covered (coefficient K, see below) was used to estimate the technique's effectiveness. The validity of the planar simplication of the three-dimensional motion of the skater is discussed in Appendix 3.

Kinematic parameters of the speed skater model

The data given by Doctorevitch (1976) were used to define the kinematic characteristics of the speed skater's run. The stroke length, the durations of the phases and the average speed in the phases were defined in these investigations. Summary data are given in Table 2.

The cubic spline method (Alberg *et al.*, 1967) was used to estimate the velocities of the skater's body segments. The speed skater's boundary positions (see Fig. 3), corresponding to the beginning of the different phases of the run, were determined in accordance with

Table 2 Kinematic characteristics of speed skating and the model on the straight part of the track

	Kinematics of running			Rhythm of running		
Manner of running	Step length (m)	Time (s)	Average speed (m s^{-1})	Free skate (t%)	Single support (t%)	Double support (t%)
Data of Doctorevitch (1976)						
Sprint events	5.05	0.42	12.0	23	49	28
	7.90	0.64	12.9			
Running on the middle distances	6.00	0.50	11.0	25	50	25
	8.40	0.70	12.1			
Running on the long distances	7.00	0.60	10.8	28	46	26
	9.20	0.80	11.5			
Model 80 push-offs per minute	8.1	0.742	10.9	27	48	25
Model 85 push-offs per minute	7.77	0.700	11.1	31.4	37.1	31.5

Note: Rhythm of running obtained by dividing the time of phase by the time of step.

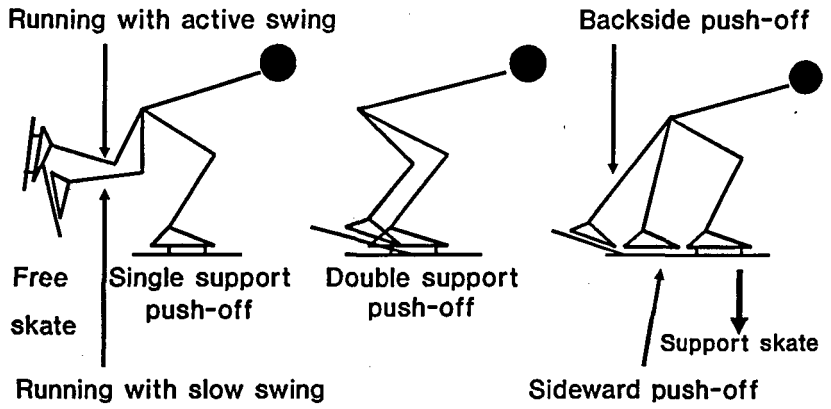

Figure 3 Variants of the technique when running on the straight parts of the circuit.

the data given in Table 2. In order that the boundary conditions between phases did not significantly influence the calculation of the velocities and accelerations, the interpolation spline was based on nine knots for each joint. In Fig. 3, stick figures are presented only for the stroke investigated. For calculating kinematic parameters, three phases were added to the right and to the left from the stroke to obtain nine knots in the joint's trajectory.

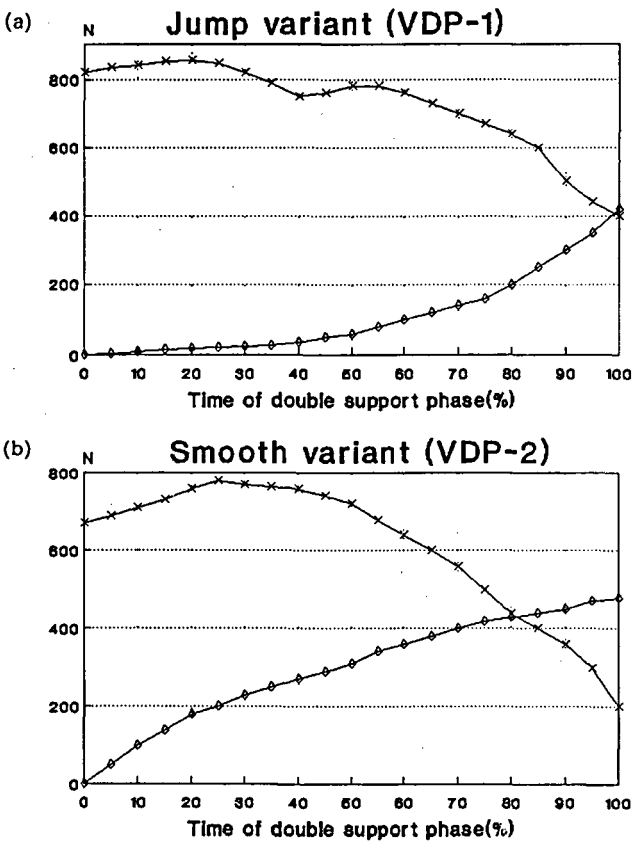

Figure 4 Vertical component (Rz) of the reaction force on the push-off (×) and support (◇) leg in the double support phase.

Simulation of the double support phase

Any system of equations has a unique solution if the number of unknowns is identical to the number of equations. The vector **W** has 11 unknowns, of which 10 are joint moments and Mr_1 is the reaction moment on the push-off leg. In vector **R**, there are five unknowns: Ry_1, Rz_1 for the push-off leg and Mr_2, Ry_2, Rz_2 for the support leg. Altogether, there are 13 equations and 16 unknowns: 10 net joint moments, 2 reaction moments and 4 reaction force components, of which 2 are along the Y axis and two along the Z axis (the directions of the Y and Z axes are shown in Fig. 2).

The given system of equations can be solved analytically only for the single support phase. In order to solve the task generally – that is, to obtain moments not only in the single support phase but in the double support phase as well (when both legs are on the ice) – it is necessary to determine the reaction moment and force components on both legs.

To obtain the force components Rz on the push-off and support legs, the following experiment was performed. The speed skater simulated the run on the straight on a skateboard. Two force platforms under the skateboard measured the force components in the double support phase. In this experiment, four speed skaters took part, each making 40 pushing attempts in the double support phase. The variation of the reaction force components on both legs is shown in Fig. 4.

According to the experiment on the skateboard, two variants of the double support phase were defined. The moving of the body weight to the support leg at the end of the double support phase (Fig. 4a) is called the 'jump' double support push-off; and the weight shift to the support leg at the beginning of the double support phase is called the 'smooth' push-off (Fig. 4b).

In calculating the ground reaction force, these two variants of executing the body movements during the double support phase have been simulated (see Fig. 5). The shift of the body weight to the support leg in the way shown in the lower line in Fig. 5a is called the first variant of the double support phase, VDP-1 (the 'jump'

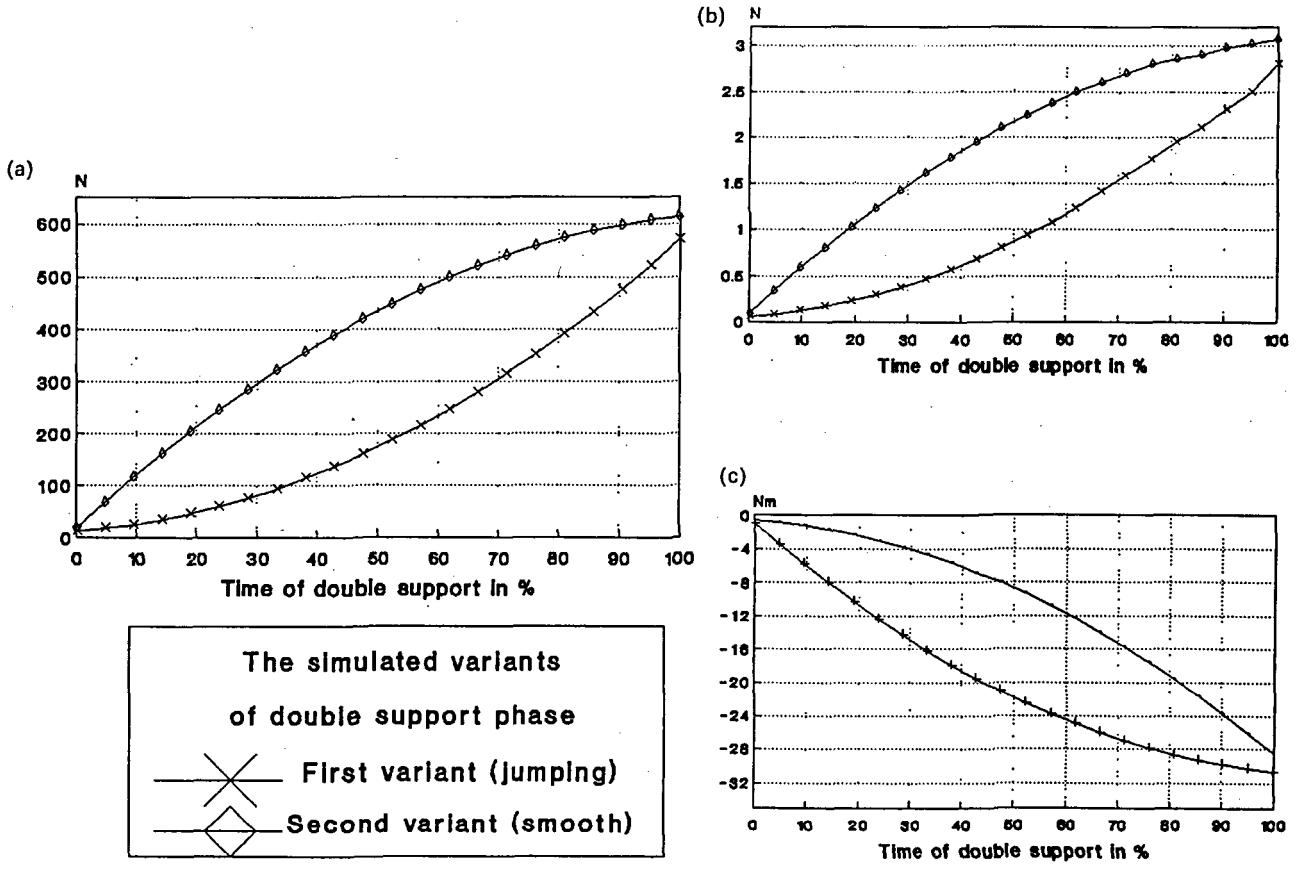

Figure 5 (a) Vertical component (Rz) of the reaction force on the support leg in the model; (b) horizontal component (Ry) of the reaction force in the model; (c) reaction moment (Mr) on the support leg.

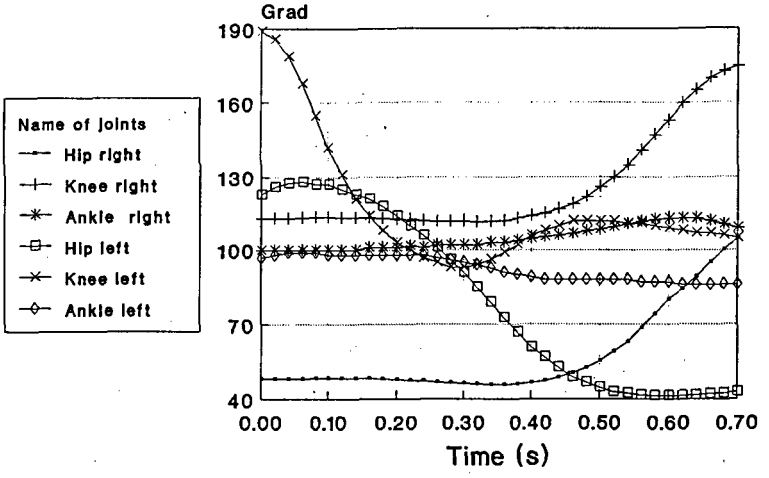

Figure 6 Joint angles where the right leg is the support push-off leg and the left leg is the swing-support leg.

variant of the double support phase), whereas that according to the upper line is the 'smooth' variant of the double support push-off, VDP-2. For these two variants of the double support phase, the vertical Rz and horizontal Ry components (see Fig. 5b) of the reaction force are given by the formulae:

$$Rz_2^{\text{VDP-1}} = (0.00006703 * \tau^2 + 0.000551 * \tau + 0.0122) * \text{weight} \quad (5)$$

$$Rz_2^{\text{VDP-2}} = (-0.00006793 * \tau^2 + 0.015178 * \tau - 0.0442) * \text{weight} \quad (6)$$

$$Ry_2 = Rz_2^{\text{VDP-1,VDP-2}} * \text{friction coefficient of ice} \quad (7)$$

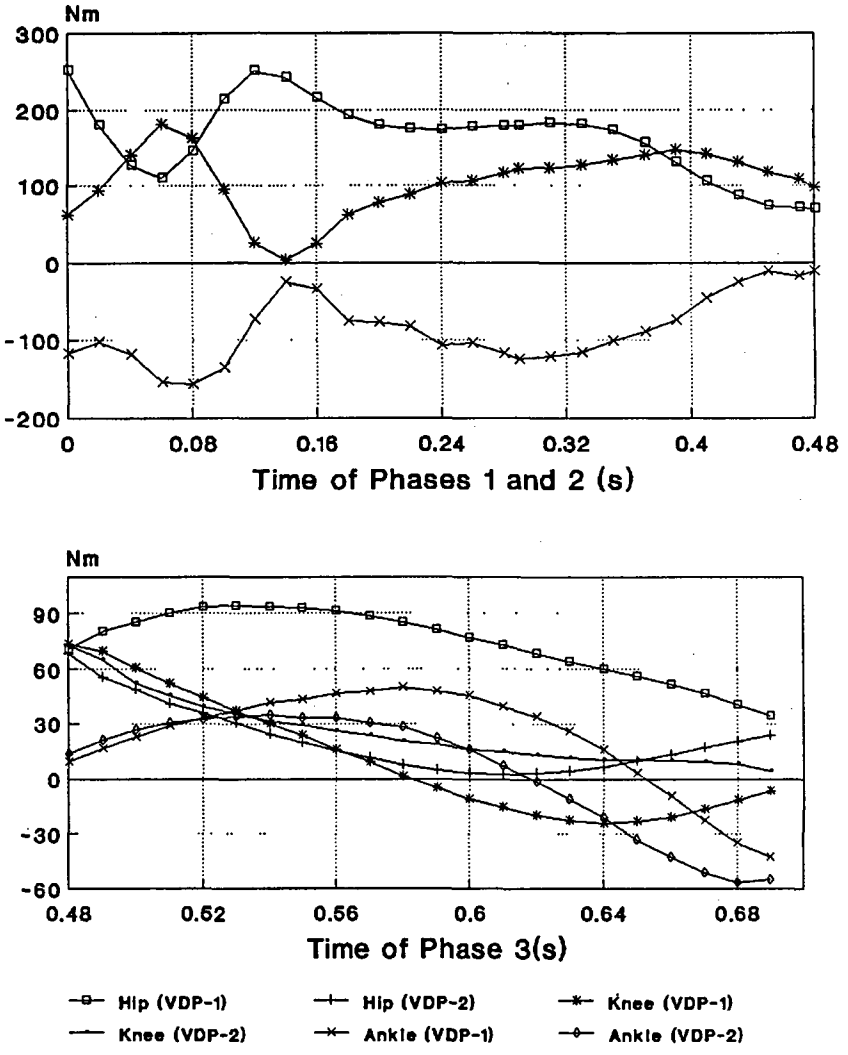

Figure 7 Joint moments and the effect of the double support push-off variant (support push-off leg).

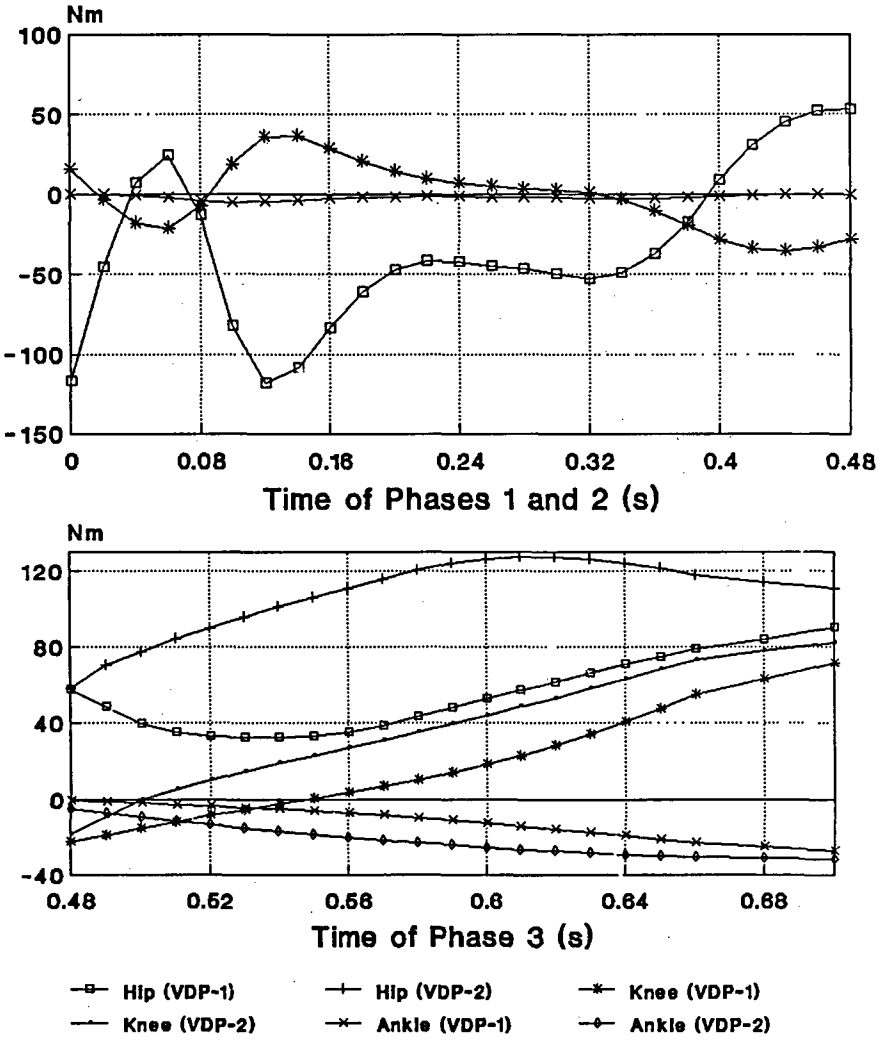

Figure 8 Joint moments and the effect of the double support push-off variant (swing-support leg).

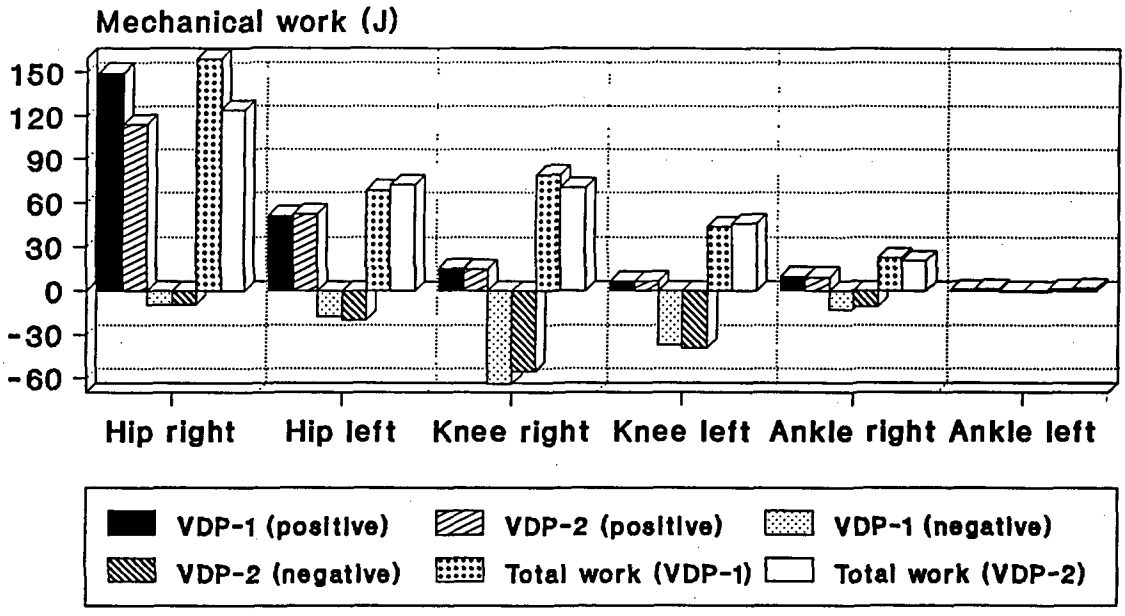

Figure 9 The mechanical work at the joints and the effect of the variant of the double support phase. Total work = 375.5 J (+232.8, −141.7, VDP-1); 334 J (+197.8, −136.2, VDP-2).

where $\tau = t_i/T$ (T is the duration of the double support phase, t_i is the instantaneous time), and the friction coefficient of ice in this model is equal to 0.005. It is necessary to point out that equation (7) is suitable only for the gliding skate.

The reaction moment on the support leg (Mr_2, see Fig. 5c) was calculated assuming that the point of force application (point of zero-moment, ZMP) lies in front of the ankle joint at a distance of 0.05 m along the surface of the blade:

$$Mr_2 = \sqrt{[Ry_2^2 + Rz_2^2]} * ZMP \qquad (8)$$

where ZMP is the position of the zero-moment point (point of force application) relative to the ankle joint.

Results and discussion

Comparative analysis of the push-off efficiency in two variants of the double support phase

To estimate the influence of the way of performing the double support phase on the joint moments and, consequently, on mechanical energy expenditure, two variants of the double support push-off (VDP-1 and VDP-2, step frequency 85 push-offs per minute) were considered (the ways of modelling body weight shifts on the support leg are illustrated in Fig. 5a–c).

The average speed in the step is 11.1 m s^{-1}. The free skate phase ends at 0.22 s; the single support phase begins at 0.22 s and ends at 0.48 s; the double support phase begins at 0.48 s and ends at 0.70 s. Figure 6 shows the angular kinematics of the stroke investigated.

The influence of the possible variants of the double support phase on the moments of the push-off and swing-support leg is shown in Figs 7 and 8. The joint moments (push-off and swing-support legs) do not depend on the modelling variant of the double support phase (VDP-1 or VDP-2) in the free skate and single support push-off phases (phases 1 and 2 in Figs 7 and 8). Hence, in the upper panels of Figs 7 and 8, there are only moment diagrams for skating with the VDP-1 variant of the double support phase.

The weight shift on the support leg according to the smooth variant (VDP-2) decreases the magnitude of the moments at the hip and ankle joints of the push-off leg (see Fig. 7). The hip moment decreases approximately four times in VDP-2 relative to VDP-1. The differences in the ankle joint moment reach a value of 35 N · m. In the variants of the double support phase investigated, the knee joint moment decreased from 50 to −20 N · m (VDP-1) or 10 N · m (VDP-2). At this period of the double support phase, the angular velocity of knee extension reaches a value of 4–5 rad s^{-1}. Hence the quadriceps femoris cannot produce a great force, and the negative value of the knee joint moment means that the moments of the (mostly two-joint) hamstring and gastrocnemius muscles are greater than the moment produced by the quadriceps femoris.

The moments Q_2, U_2 and P_2 in the support leg joints are greater in VDP-2 then when the first variant of the double support phase (VDP-1) takes places (see Fig. 8). In the variants of running simulated with two different

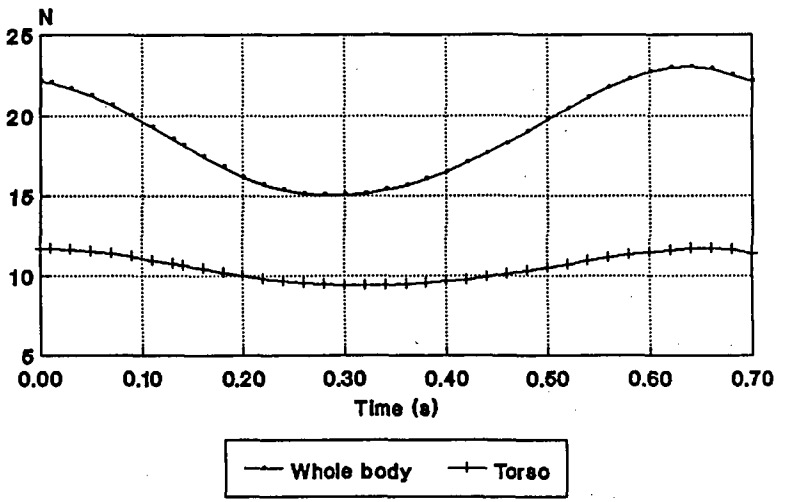

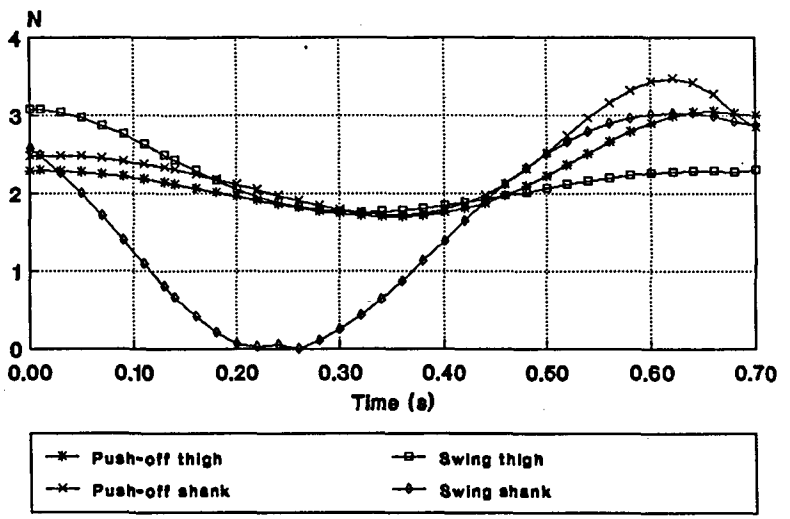

Figure 10 Aerodynamic forces acting on the skater's body segments (wind speed = 0 m s^{-1}).

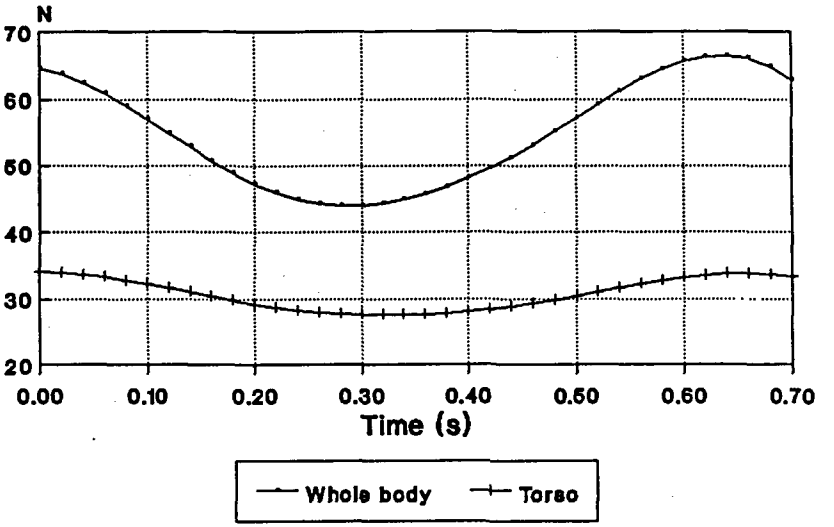

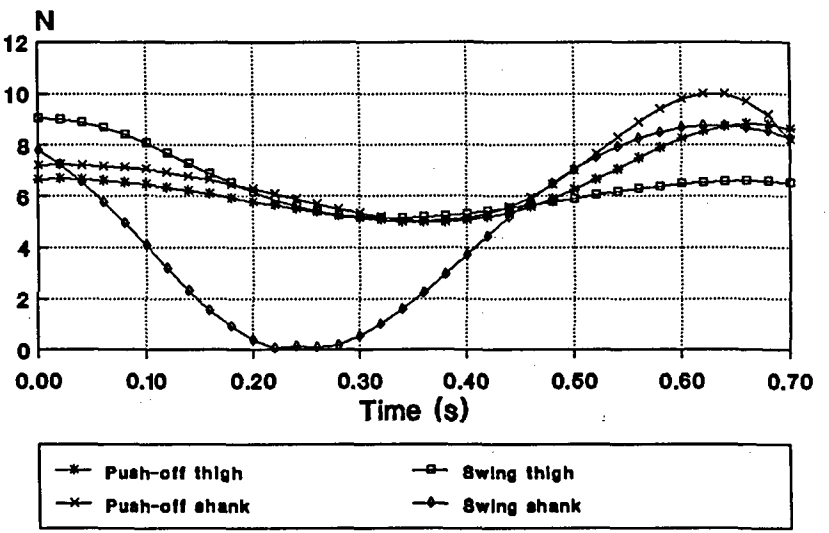

Figure 11 Aerodynamic forces acting on the skater's body segments (wind speed = 8 m s^{-1}).

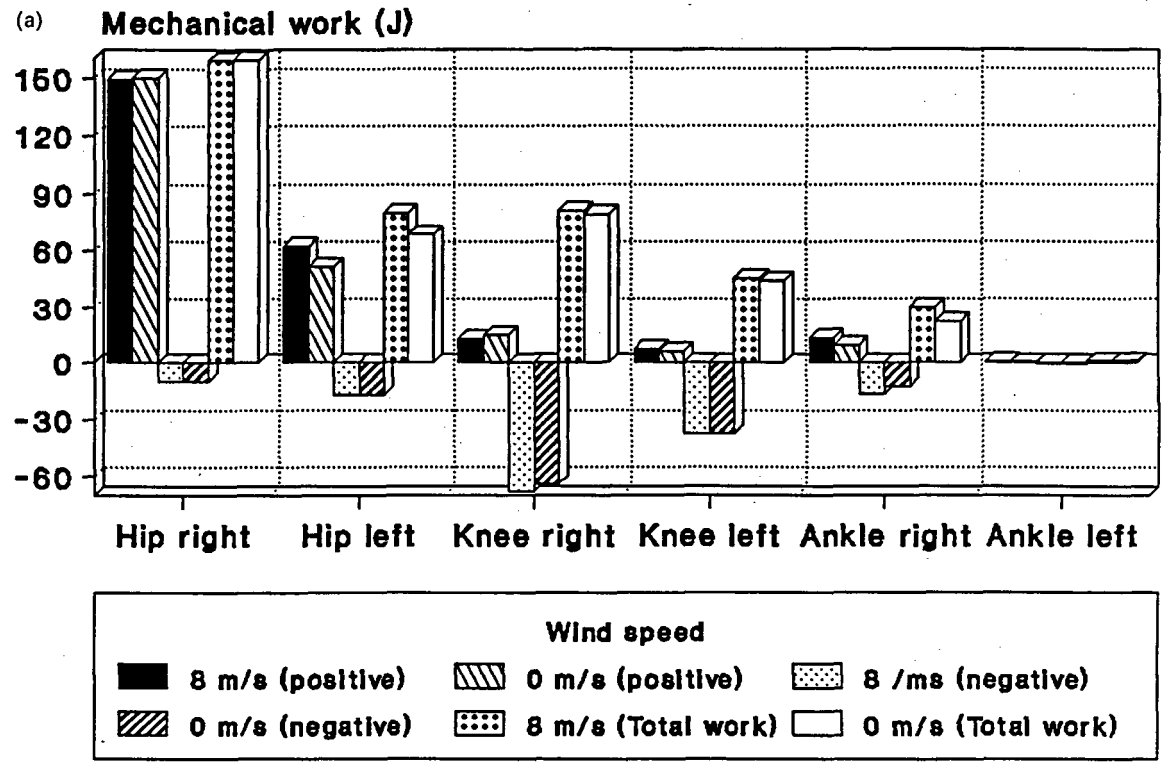

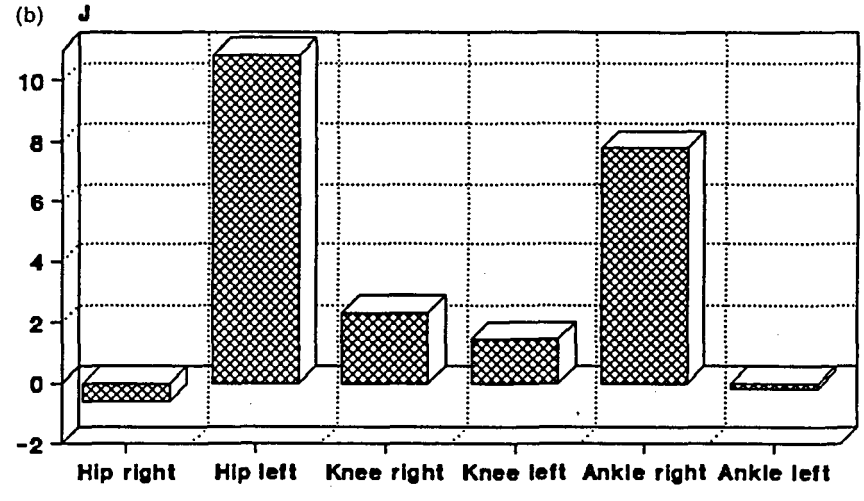

Figure 12 (a) The influence of air resistance on mechanical energy expenditure; (b) the difference in total mechanical energy expenditure in the joints as a function of air resistance.

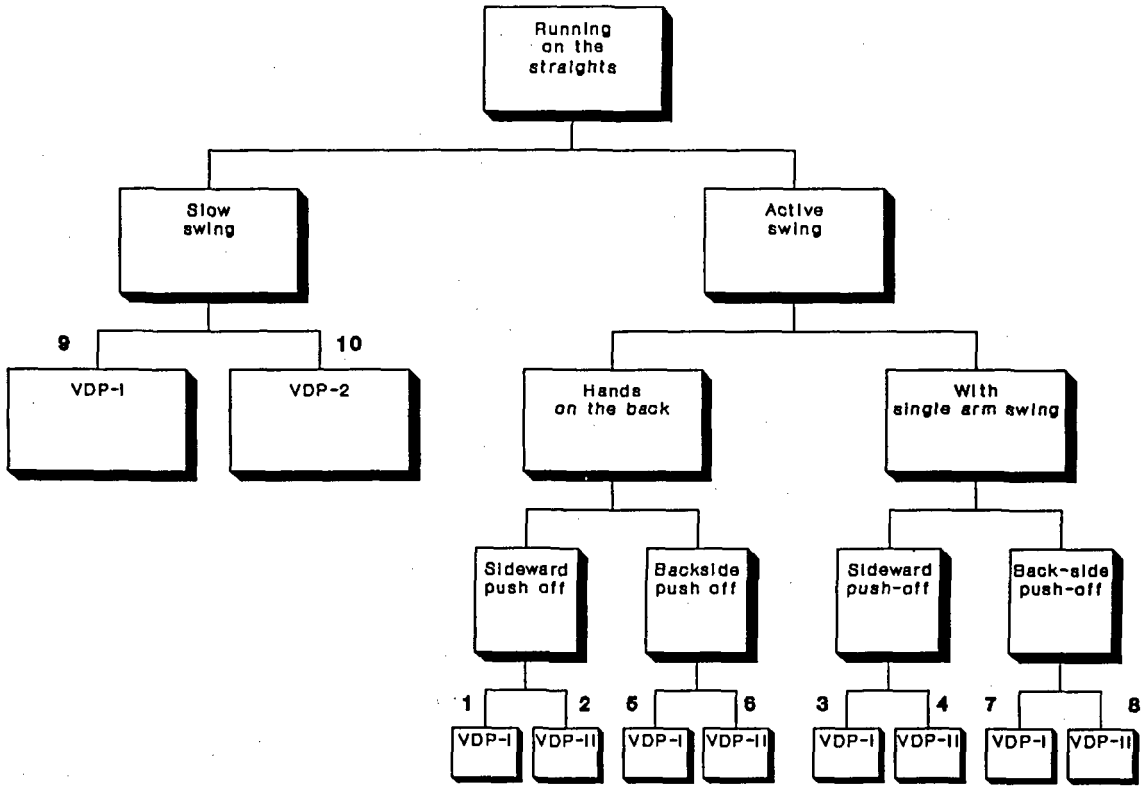

Figure 13 A schematic representation of the different simulations for speed skating.

weight shifts on the support leg in phase 3, the run under the VDP-2 is more effective: at a frequency of 85 steps per min, the work output per metre decreases from 48.2 to 43.0 J m^{-1} (under VDP-2) or by 10.8% (see Fig. 9).

So the 'smooth' double support push-off (VDP-2) seems to be more effective than the 'jump' (VDP-1). This can be explained by the fact that the mechanical work (equation 4) is the product of two variables: the joint moment and angular displacement. The angular displacement of the support leg joints in phase 3 is negligible relative to the joint displacements of the push-off leg (see Fig. 6), so the mechanical work in the support leg joints in the double support phase is approximately equal to zero in VDP-1 and VDP-2. The decrease in the work of the push-off leg decreases the total mechanical work in the step. Under the same speed of running, the skater who 'loads' the support leg earlier, expends less mechanical energy.

The influence of aerodynamic drag on power and mechanical energy expenditure of the speed skater

The aerodynamic forces acting on the segments are shown in Figs 10 and 11, the average speed in the step being about 11.1 m s^{-1}. The drag forces acting on the segments are presented in Fig. 10, where the velocity of the opposing wind V is equal to zero. If the velocity of the wind increases to 8 m s^{-1}, then the drag force increases in the manner presented in Fig. 11. In that case, the velocity of the hip joint in phase 1 changes: the increase in drag force should decrease the speed in the free-skate phase. The impulse of drag forces according to Fig. 11 in phase 1 (0–0.22 s) is 12 N s^{-1}, so the average speed of the skater (body mass 78.7 kg) decreases to the end of the free-skate phase by 0.15 m s^{-1}.

The effect of wind speed on the mechanical work in the joints is presented in Fig. 12. The rise in wind speed from 0 to 8 m s^{-1} increases the mechanical work in the step from 375 to 396 J (VDP-1) and decreases the technique efficiency of skating by 5.8%.

The simulation of different versions of the running technique on the straight part of the circuit and the estimation of their efficiency

For this purpose, 10 new middle-stroke running versions were considered. They are numbered in the columns of Table 3 and Fig. 13. The main differences in touch-down positions concern the position of the push leg and the swing leg relative to the hip joint. The average speed (10.9 m s^{-1}) of the hip joint, the stride frequency of 80 strokes per min and phase structure remain the same in all 10 versions, with the wind speed equal to zero. A general overview of the versions considered is presented in Fig. 13.

Table 3 Mechanical energy expenditure (J) on the straight part of the track (80 strokes per min)

Work and errors of model	Running with sideward push-off with active swing			
	Variant 1: Hands on the back, VDP-1	Variant 2: Hands on the back, VDP-2	Variant 3: Single arm swing, VDP-1	Variant 4: Single arm swing, VDP-2
Mechanical work in step[a]				
total	393	312	419	334
positive	252	197	259	200
negative	141	115	160	134
Work of aerodynamic forces	138	138	150	150
The error of the planar model (%)	6.8	17.9	12.3	24.8
K (J m^{-1})	48.5	38.5	51.7	41.3
	Running with sideward push-off with active swing			
Work and errors of model	Variant 5: Hands on the back, VDP-1	Variant 6: Hands on the back, VDP-2	Variant 7: Single arm swing, VDP-1	Variant 8: Single arm swing, VDP-2
Mechanical work in step[a]				
total	462	351	487	375
positive	271	206	277	211
negative	191	145	211	165
Work of aerodynamic forces	138	138	150	150
The error of the planar model (%)	12.2	22.2	17.2	27.7
K (J m^{-1})	57.0	43.4	60.1	42.3
	Running with sideward push-off without active swing			
Work and errors of model	Variant 9: Hands on the back, VDP-1	Variant 10: Hands on the back, VDP-2		
Mechanical work in step[a]				
total	262	239		
positive	188	171		
negative	73.5	68.0		
Work of aerodynamic forces	139	139		
The error of the planar model (%)	9.2	14.9		
K (J m^{-1})	32.3	29.5		

Note: The work done against aerodynamic resistance was obtained by multiplying resistance force by the step length.
[a] Total, positive and negative work at the joints.

The model assumes constant length of segments (rigid bodies), so in simulating procedures when the 'back-side' push-off occurs, the angle of thigh inclination to the vertical (β_1; see Fig. 2) alters, until the toe of the blade touches the ice at the end of the double support phase (see Fig. 3).

The double support push-off is modelled by two possible variants of the body weight shift on the support leg (see Fig. 5). The estimation of the efficiency of the technique is defined by the coefficient K (the work done per metre of the distance travelled). The total mechanical work per stroke and the coefficient K are shown in Table 3. The total mechanical energy expenditure in the back-side push-off (variants 5–8) in comparison with sideward push-off (variants 1–4) increases by 17% under VDP-1 and by 13% under VDP-2.

The amplitude and 'activity' of motion of the swing leg (variants 1–8 *vs* 9–10) essentially affect the reaction force component along the Y axis. This is explained by the fact that the direction of the centre of mass acceleration of the swing leg does not coincide with the direction of the support leg centre of mass. When the swing leg touches the ice (deceleration), the negative forces act on the skater's centre of mass. Hence the push-off leg develops more mechanical work to maintain the given velocity in the step.

For running with an active swing, the mechanical work equals 393 J (variant 1, VDP-1) and 312 J (variant 2, VDP-2); skating with back-side push-off increases the mechanical work in the joints to 462 J (variant 5, VDP-1) and 350 J (variant 6, VDP-2). When skating without an active leg swing and with sideward push-off (variants 9 and 10), the mechanical work in the push-off leg joints equals 262 J (variant 9, VDP-1) and 239 J

(variant 10, VDP-2). In all variants of running, the mechanical efficiency rises by 20–30% if variants with VDP-2 are used (compare pairs 1–2, 3–4, 5–6, etc.).

The energy used for the arm swing does not exceed 5% of the total energy expenditure and does not essentially affect the general efficiency (variant 1–2 *vs* 3–4 and 5–6 *vs* 7–8). The swinging of the arm increases the energy expenditure per metre of distance travelled by 3 J m^{-1} under all variants.

The most effective technique at the step frequency studied (80 steps per min) is the run without arms swinging, with a sideward push-off and without an active swing by the recovery leg (variant 10, $K=$ 29.5 J m^{-1}).

Conclusions

The analysis of the movement of a speed skater on the straight part of the circuit on the basis of a planar 11-segment mechanical model has shown:

1. The system of equations describing the movement of a speed skater on the straight part of the lap has a unique solution for the single support position, while in the double support phase the system is indeterminate.
2. The use of the second variant of the double support push-off (VDP-2) decreases the mechanical energy expenditure per stroke by 10–30%. Therefore, it is recommended that the skater should place the recovery leg on the ice and 'load' it as early as possible.
3. The rise of opposing wind speed from 0 to 8 m s^{-1} increases the average air resistance force from ~20 to ~55 N and decreases the technique efficiency by 5.8%. The total mechanical energy expenditure increases with the rise of air resistance by 11 J for the swing hip and by 7 J for the push-off ankle.
4. Sideward push-off with a small magnitude of the swing movement (variants 9 and 10, Table 3) reduces the negative value of the horizontal reaction force in the final part of the single support push-off. The mechanical energy expenditure in the step decreases in this case by a factor of 1.5.
5. The most efficient technique (variant 10, Table 3) was found to be the run without arm swing, with a sideward push-off and without an active swing by the recovery leg, which reduces the mechanical work rate to 29.5 J m^{-1}.

Acknowledgements

The authors wish to thank V.N. Selujanov, senior scientific associate of GTsOLIFK, for his interest and advice during the preparation of the manuscript, as well as G.V. Judin, Z.N. Belyakova and A.O. Minnenkov for their invaluable assistance in the acquisition of the aerodynamic data. The authors also wish to thank Professor Roger Bartlett for his valuable advice and attention in preparation of the manuscript.

References

Alberg, J.H., Nilson, E.N. and Walsh, J.L. (1967). *The Theory of Splines and Their Applications*. New York: Academic Press.

Beletsky, V.V. (1984). *Bipedal Walking*. Moscow: Nauka (in Russian).

de Boer, R.W. (1986). Training and technique in speed skating (a biomechanical and exercise physiological study). Unpublished doctoral dissertation, Free University Amsterdam.

Di Prampero, P.E., Cortili, G., Mognoni, P. and Saibine, F. (1976). Energy cost of speed skating and efficiency of work against air resistance. *Journal of Applied Physiology*, **40**, 584–591.

Doctorevitch, M.V. (1976). Analysis of kinematic and dynamic characteristics in speed skating. *Speed Skating Sport*, **2**, 48–54 (in Russian).

Ekblom, B., Hermansen, L. and Saltin, B. (1967). Hastighetsakning paskridskor. Idrottsfysiologi Rapport No. 5.

Formalsky, A.M. (1982). *Movement of the Anthropomorphic Mechanism*. Moscow: Nauka (in Russian).

Kandow, T.W.A., Houtman, I.I.D., Bol, E.V.D., de Boer, R.W., de Groot, G. and van Ingen Schenau, G.J. (1987). Comparison of physiology and biomechanics of speed skating with cycling and with skate board exercise. *Canadian Journal of Sport Science*, **12**, 31–36.

Koning, J.J., de Groot, G. and van Ingen Schenau, G.J. (1991a). Coordination of leg muscles during speed skating. *Journal of Biomechanics*, **24**, 137–146.

Koning, J.J., de Groot, G. and van Ingen Schenau, G.J. (1991b). Speed skating the curves: A study of muscle coordination and power production. *International Journal of Sport Biomechanics*, **7**, 344–358.

Sokolov, M.P. (1970). The leading elements of speed skaters' technique. *Theory and Practice of Physical Culture*, **1**, 30–36 (in Russian).

van Ingen Schenau, G.J. (1981). A power balance applied to speed skating. Unpublished doctoral dissertation, Free University Amsterdam.

Zatsiorsky, V.M. and Prilutsky, B.I. (1986). *Physiology of Negative Work*. Moscow: GTsOLIFK (in Russian).

Zatsiorsky, V.M., Aleshinsky, S.J. and Yakunin, N.A. (1982). *Biomechanical Basis of Endurance*. Moscow: Physical Culture and Sport (in Russian).

Zatsiorsky, V.M., Aruin, A.S. and Selujanov, V.N. (1981). *Biomechanics of the Musculo-skeletal System*. Moscow: Physical Culture and Sport (in Russian).

Appendix 1

- $\ddot{\lambda}=[\ddot{Y}^0, \ddot{Z}^0, \ddot{\alpha}, \ddot{\beta}_1, \ddot{\beta}_2, \ddot{\gamma}_1, \ddot{\gamma}_2, \ddot{\eta}_1, \ddot{\eta}_2, \ddot{\xi}_1, \ddot{\theta}_1, \ddot{\xi}_2, \ddot{\theta}_2]^T$
- $\sin(\lambda)=[0, 1, \sin(\alpha), \sin(\beta_1), \sin(\beta_2), \sin(\gamma_1), \sin(\gamma_2), \sin(\eta_1), \sin(\eta_2), \sin(\xi_1), \sin(\theta_1), \sin(\xi_2), \sin(\theta_2)]^T$
- $\dot{\lambda}^2=[0, 0, \dot{\alpha}^2, \dot{\beta}_1^2, \dot{\beta}_2^2, \dot{\gamma}_1^2, \dot{\gamma}_2^2, \dot{\eta}_1^2, \dot{\eta}_2^2, \dot{\xi}_1^2, \dot{\theta}_1^2, \dot{\xi}_2^2, \dot{\theta}_2^2]^T$
- $\mathbf{W}=[0, 0, Q_1, Q_2, U_1, U_2, P_1, P_2, Mr_1, S_1, \tau_1, S_2, \tau_2]^T$
- $\mathbf{R}=[Ry_1, Rz_1, Mr_2, Ry_2, Rz_2, -F^a, -F_T^a, -F_{Th1}^a, -F_{Th2}^a, -F_{Sh1}^a, -F_{Sh2}^a, 0, 0]^T$
- DIAG $C=[0, m, -A_1, B_1, B_1, C_1, C_1, K_F, K_F, D_1, K_{La}, D_1, K_{La}]$

where:

Q_i = the hip joint moments (see Fig. 2), U_i the knee joint moments, P_i the ankle joint moments, S_i the shoulder joint moments and τ_i the elbow joint moments;
Ry_i, Rz_i = the horizontal and vertical reaction force components;
Mr_i = the reaction moments relative to the ankle joint;
F^a = air resistance (with no suffix: air resistance of the skater's body; with suffices indicating: T, air resistance of torso plus head; Th, air resistance of thigh; Sh, air resistance of shank plus foot plus skate);
m = body mass of skater.

Coefficients of matrix A, B, C, D, E

- $K_T=m_T*R_T$: $K_{Th}=m_{Th}*R_{Th}$: $K_{Sh}=m_{Sh}*R_{Sh}$: $K_F=m_F*R_F$: $K_{Ua}=m_{Ua}*R_{Ua}$: $K_{La}=m_{La}*R_{La}$
- $P_1=K_{Th}+L_{Th}*(m_{Sh}+m_F)$: $P_2=K_{Sh}+m_F*L_{Sh}$: $P_3=K_{Ua}+m_{La}*L_{Ua}$: $P_4=K_T+2*L_T*(m_{La}+m_{Ua})$
- $A_1=P_4$: $A_2=L_T*(K_{Ua}+m_{La}*L_{Ua})$: $A_3=\mathcal{J}_T+2*L_T^2*(m_{Ua}+m_{La})$
- $B_1=K_{Th}+L_{Th}*(m_{Sh}+m_F)$: $B_2=L_{Th}*(K_{Sh}+m_F*L_{Sh})$: $B_3=\mathcal{J}_{Th}+L_{Th}^2*(m_{Sh}+m_F)$
- $C_1=K_{Sh}+m_F*L_{Sh}$: $C_2=\mathcal{J}_{Sh}+m_F*L_{Sh}^2$
- $D_1=K_{Ua}+m_{La}*L_{Ua}$: $D_2=\mathcal{J}_{Ua}+m_{La}*L_{Ua}^2$
- $\mathcal{J}_T=\mathcal{J}_T^0+m_T*R_T^2$: $\mathcal{J}_{Th}=\mathcal{J}_{Th}^0+m_{Th}*R_{Th}^2$: $\mathcal{J}_{Sh}=\mathcal{J}_{Sh}^0+m_{Sh}*R_{Sh}^2$: $\mathcal{J}_F=\mathcal{J}_F^0+m_F*R_F^2$: $\mathcal{J}_{Ua}=\mathcal{J}_{Ua}^0+m_{Ua}*R_{Ua}^2$: $\mathcal{J}_{La}=\mathcal{J}_{La}^0+m_{La}*R_{La}^2$

where:
m = segment mass;
$\mathcal{J}^0$ = the moment of inertia of the segment relative to its centre of mass (or centre of mass of torso for $\mathcal{J}_T^0$);
segment suffices are: T, torso plus head; Th, thigh; Sh, shank; F, foot; Ua, upper arm; La, lower arm plus hand;
L = segment length with suffices as above except L_T is torso length from hips to shoulders;
R_T = distance between the proximal joint (hip) and the torso plus head centre of mass;
R_{Th} = distance between the proximal joint (hip) and the thigh centre of mass;
R_{Sh} = distance between the proximal joint (knee) and the shank centre of mass;
R_F = distance between the proximal joint (ankle) and the foot centre of mass;
R_{Ua} = distance between the proximal joint (shoulder) and the upper arm centre of mass;
R_{La} = distance between the proximal joint (elbow) and the lower arm plus hand centre of mass.

Coefficients of matrix A (matrix A is symmetrical)

- $A(1,1)=m$: $A(1,2)=0$: $A(1,3)=P_4*\cos(\alpha)$: $A(1,4)=P_1*\cos(\beta_1)$: $A(1,5)=P_1*\cos(\beta_2)$: $A(1,6)=-P_2*\cos(\gamma_1)$: $A(1,7)=-P_2*\cos(\gamma_2)$: $A(1,8)=K_F*\cos(\eta_1)$: $A(1,9)=K_F*\cos(\eta_2)$: $A(1,10)=P_3*\cos(\xi_1)$: $A(1,11)=K_{La}*\cos(\theta_1)$: $A(1,12)=P_3*\cos(\xi_2)$: $A(1,13)=K_{La}*\cos(\theta_2)$
- $A(2,2)=m$: $A(2,3)=-P_4*\sin(\alpha)$: $A(2,4)=P_1*\sin(\beta_1)$: $A(2,5)=P_1*\sin(\beta_2)$: $A(2,6)=P_2*\sin(\gamma_1)$: $A(2,7)=P_2*\sin(\gamma_2)$: $A(2,8)=K_F*\sin(\eta_1)$: $A(2,9)=K_F*\sin(\eta_2)$: $A(2,10)=P_3*\sin(\xi_1)$: $A(2,11)=K_{La}*\sin(\theta_1)$: $A(2,12)=P_3*\sin(\xi_2)$: $A(2,13)=K_{La}*\sin(\theta_2)$
- $A(3,3)=A_3$: $A(3,4)=A(3,5)=A(3,6)=A(3,7)=A(3,8)=A(3,9)=0$: $A(3,10)=A_2*\cos(\alpha+\xi_1)$: $A(3,11)=K_{La}*L_T*\cos(\alpha+\theta_1)$: $A(3,12)=A_2\cos(\alpha+\xi_2)$: $A(3,13)=K_{La}*L_T*\cos(\alpha+\theta_2)$
- $A(4,4)=B_3$: $A(4,5)=0$: $A(4,6)=-B_2*\cos(\gamma_1+\beta_1)$: $A(4,7)=0$: $A(4,8)=K_F*L_{Th}*\cos(\beta_1-\eta_1)$: $A(4,9)=A(4,10)=A(4,11)=0$: $A(4,12)=A(4,13)=0$
- $A(5,5)=B_3$: $A(5,6)=0$: $A(5,7)=-B_2*\cos(\gamma_2+\beta_2)$: $A(5,8)=0$: $A(5,9)=K_F*L_{Th}*\cos(\beta_2-\eta_2)$: $A(5,10)=A(5,11)=A(5,12)=A(5,13)=0$
- $A(6,6)=C_2$: $A(6,7)=0$: $A(6,8)=-K_F*L_{Sh}*\cos(\gamma_1+\eta_1)$: $A(6,9)=A(6,10)=A(6,11)=A(6,12)=A(6,13)=0$
- $A(7,7)=C_2$: $A(7,8)=0$: $A(7,9)=-K_F*L_{Sh}*\cos(\gamma_2+\eta_2)$: $A(7,10)=A(7,11)=A(7,12)=A(7,13)=0$
- $A(8,8)=\mathcal{J}_F$: $A(8,9)=A(8,10)=A(8,11)=A(8,12)=A(8,13)=0$
- $A(9,9)=\mathcal{J}_F$: $A(9,10)=A(9,11)=A(9,12)=A(9,13)=0$

- $A(10, 10)=D_2$: $A(10, 11)=K_{La}*L_{Ua}*\cos(\theta_1-\xi_1)$: $A(10, 12)=A(10, 13)=0$
- $A(11, 11)=\mathcal{J}_{La}$: $A(11, 12)=A(11, 13)=0$
- $A(12, 12)=D_2$: $A(12, 13)=K_{La}*L_{Ua}*\cos(\theta_2-\xi_2)$
- $A(13, 13)=\mathcal{J}_{La}$

Coefficients of matrix B (first two columns of matrix B are zero)

- $B(1, 3)=-P_4*\sin(\alpha)$: $B(1, 4)=-P_1*\sin(\beta_1)$: $B(1, 5)=-P_1*\sin(\beta_2)$: $B(1, 6)=P_2*\sin(\gamma_1)$: $B(1, 7)=P_2*\sin(\gamma_2)$: $B(1, 8)=-K_F*\sin(\eta_1)$: $B(1, 9)=-K_F*\sin(\eta_2)$: $B(1, 10)=-P_3*\sin(\xi_1)$: $B(1, 11)=-K_{La}*\sin(\theta_1)$: $B(1, 12)=-P_3*\sin(\xi_2)$: $B(1, 13)=-K_{La}*\sin(\theta_2)$
- $B(2, 3)=-P_4*\cos(\alpha)$: $B(2, 4)=P_1*\cos(\beta_1)$: $B(2, 5)=P_1*\cos(\beta_2)$: $B(2, 6)=P_2*\cos(\gamma_1)$: $B(2, 7)=P_2*\cos(\gamma_2)$: $B(2, 8)=K_F*\cos(\eta_1)$: $B(2, 9)=K_F*\cos(\eta_2)$: $B(2, 10)=P_3*\cos(\xi_1)$: $B(2, 11)=K_{La}*\cos(\theta_1)$: $B(2, 12)=P_3*\cos(\xi_2)$: $B(2, 13)=K_{La}*\cos(\theta_2)$

From the third column and row, matrix B is symmetrical except for the following elements:

- $B(4, 8)=-B(8, 4)$: $B(5, 9)=-B(9, 5)$: $B(10, 11)=-B(11, 10)$: $B(12, 13)=-B(13, 12)$

The non-zero elements of matrix B beginning from the third column and third row are:

- $B(3, 10)=-A_2*\sin(\alpha+\xi_1)$: $B(3, 11)=-K_{La}*L_T*\sin(\alpha+\theta_1)$: $B(3, 12)=-A_2*\sin(\alpha+\xi_2)$: $B(3, 13)=-K_{La}*L_T*\sin(\alpha+\theta_2)$
- $B(4, 6)=B_2*\sin(\gamma_1+\beta_1)$: $B(4, 8)=K_F*L_{Th}*\sin(\beta_1-\eta_1)$
- $B(5, 7)=B_2*\sin(\gamma_2+\beta_2)$: $B(5, 9)=K_F*L_{Th}*\sin(\beta_2-\eta_2)$
- $B(6, 8)=K_F*L_{Sh}*\sin(\gamma_1+\eta_1)$
- $B(7, 9)=K_F*L_{Sh}*\sin(\gamma_2+\eta_2)$
- $B(10, 11)=-K_{La}*L_{Ua}*\sin(\theta_1-\xi_1)$
- $B(12, 13)=-K_{La}*L_{Ua}*\sin(\theta_2-\xi_2)$

Coefficients of matrix D

$D(3, 3)=-1$: $D(3, 4)=-1$: $D(3, 10)=-1$: $D(3, 12)=-1$: $D(4, 3)=-1$: $D(4, 5)=-1$: $D(5, 4)=-1$: $D(5, 6)=-1$
$D(6, 5)=-1$: $D(6, 7)=-1$: $D(7, 6)=-1$: $D(7, 8)=-1$: $D(8, 7)=-1$: $D(8, 9)=-1$: $D(9, 8)=-1$: $D(10, 10)=-1$
$D(10, 11)=1$: $D(11, 11)=-1$: $D(12, 12)=-1$: $D(12, 13)=1$: $D(13, 13)=-1$

The other coefficients of matrix D are equal to zero.

Coefficients of matrix E

$E(1, 1)=1$: $E(1, 4)=1$: $E(1, 6)=1$: $E(2, 2)=1$: $E(2, 5)=1$: $E(3, 7)=L_T*\cos(\alpha)$: $E(4, 1)=L_{Th}*\cos(\beta_1)$: $E(4, 2)=L_{Th}*\sin(\beta_1)$
$E(4, 8)=R_{Th}*\cos(\beta_1)$: $E(4, 10)=L_{Th}*\cos(\beta_1)$: $E(5, 4)=L_{Th}*\cos(\beta_2)$: $E(5, 5)=L_{Th}*\sin(\beta_2)$: $E(5, 9)=R_{Th}*\cos(\beta_2)$
$E(5, 11)=L_{Th}*\cos(\beta_2)$: $E(6, 1)=-L_{Sh}*\cos(\gamma_1)$: $E(6, 2)=L_{Sh}*\sin(\gamma_1)$: $E(6, 10)=-R_{Sh}*\cos(\gamma_1)$: $E(7, 4)=-L_{Sh}*\cos(\gamma_2)$
$E(7, 5)=L_{Sh}*\sin(\gamma_2)$: $E(7, 11)=-R_{Sh}*\cos(\gamma_2)$: $E(9, 3)=-1$

All other coefficients of matrix E are equal to zero.

Appendix 2

Table 4 Coefficients of regression equation $C_x = A_k * v^2 + B_k * v + C_k$

Form of touch-down	A_k	B_k	C_k
Skating on the straight part of the circuit with hands on the back			
End of double support phase	0.00193	−0.05905	1.37320
Beginning of single support take-off phase	0.00338	−0.08871	1.39160
Beginning of double support phase	0.00240	−0.06278	1.19520
Skating on the straight part of the circuit with one-arm swing			
End of double support phase	0.00405	−0.10650	1.56370
Beginning of single support take-off phase	0.00513	−0.12930	1.68450
Beginning of double support phase	0.00589	−0.15350	1.95760
Skating on the straight part of the circuit with two-arm swing			
End of double support phase	0.00365	−0.09989	1.60350
Beginning of single support take-off phase	0.00378	−0.09950	1.52870
Beginning of double support phase	0.00535	−0.13644	1.90390

Table 5 Coefficients of regression equation $S = a + b * X_1 + c * X_2 + d * X_3 + e * X_4$ for calculating frontal section area of segments in touch-down (m^2)

Form of touch-down Segment	a	b	c	d	e
Frontal section of segments in beginning of single support push-off phase					
Torso	−0.04900	0.00267	−0.00157	0.00276	0.00356
Thigh (take-off)	−0.01250	0.00007	−0.00011	0.00054	0.00054
Thigh (swing)	0.02750	0.00052	0.00040	−0.00145	−0.00029
Shank (take-off)	−0.05600	−0.00010	0.00057	0.00023	−0.00018
Shank (swing)	In this phase of skating, the swing shank is approximately horizontal.				
Frontal section of segments in beginning of double support push-off phase					
Torso	−0.04900	0.00267	−0.00157	0.00276	0.00356
Thigh (take-off)	−0.01250	0.00007	−0.00011	0.00054	0.00054
Thigh (support)	−0.01250	0.00007	0.00011	−0.00054	−0.00054
Shank (take-off)	−0.05600	0.00010	0.00057	0.00023	−0.00018
Shank (support)	−0.05600	0.00010	0.00057	0.00023	−0.00018
Frontal section of segments at the end of double support push-off phase					
Torso	−0.04900	0.00267	−0.00157	0.00276	0.00356
Thigh (take-off)	−0.03790	0.00036	0.00032	−0.00043	0.00050
Thigh (support)	−0.01250	0.00007	0.00011	−0.00054	−0.00054
Shank (take-off)	−0.02200	0.00029	0.00026	−0.00023	0.00012
Shank (support)	−0.05600	0.00010	0.00057	0.00023	−0.00018

Note: X_1 = mass of the skater (kg);
X_2 = length of body (cm);
X_3 = for torso is width of shoulders (43 cm), for thigh is mean circumference (56 cm), for shank is maximum circumference (34 cm);
X_4 = angle of hip joint (60°) of push-off leg in single support or beginning of double support phase; at the end of the double support phase, this angle is that of the hip joint of the support leg.

Appendix 3

The validity of the planar simplification of the three-dimensional model

Speed skating is a typically three-dimensional (3-D) motion. But it is difficult to obtain the skater's 3-D coordinates in real running and especially to develop the 3-D model. It is possible to make some simplifications which will decrease the complexity and the size of the model, for example to develop a planar model of skating. When the 3-D model is replaced by a planar one, it is necessary to estimate the validity of such a substitution.

The push-off forces in real skating and the planar model

First, the main biomechanical features of skating on the straight parts of the circuit will be discussed. In Fig. 14, an upper view of the 3-D skater model is presented. The forward motion of the skater is possible only when the push-off force, applied to the skate, is approximately perpendicular to the blade, and the skate is turned around the Z axis in the manner shown in Fig. 14. In such a variant of the push-off, a positive reaction force component *Ry* moves the skater forwards and the component *Rx* is connected with sideward motion of the skater. The work done by the push-off forces in the step is approximately equal to zero because of the right angle between the direction of the skate's motion and the push-off force applied.

In the 3-D model, in the inertial coordinate system, the component *Ry* differs from the friction force, but in the skate's X^s, Y^s, Z^s system of coordinates, *Ry* always has a negative value (friction force). In the 2-D (planar) model, the Y axis of the skate (axis along the blade) and the direction of the Y axis of the inertial system coincide, hence differences between *Ry* and the friction force appear.

In the planar model, the *Rx* force component is always equal to zero, so it is not possible to calculate the work done to sideward skater motion. The *Rz* force in the 3-D and the 2-D models approximately equals the weight of the skater in phases 1 and 2 and rapidly decreases in phase 3.

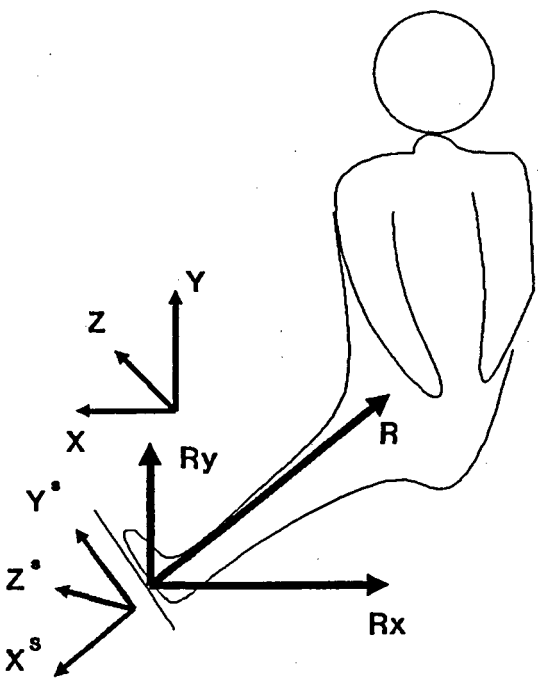

Figure 14 The upper view of the three-dimensional motion of a skater on the straight parts of the circuit. XYZ, inertial coordinate system; $X^sY^sZ^s$, 'skate' coordinate system; **R**, reaction support forces.

The balance of mechanical energy in the planar and 3-D models of skating

In the 3-D model, the difference between potential and kinetic energy at the beginning and at the end of the step is equal to the work done by the aerodynamic, reaction and friction forces and also the work of the joint moments.

In the 3-D model of the skater, the work done by the reaction forces is approximately equal to zero, hence mechanical work in the joints plus the work of aerodynamic and friction forces are equal to the change of potential and kinetic energy in the step. When the velocities of the skater's centre of mass at the beginning and the end of the step are equal (long-distance running), the difference in potential and kinetic energy of the skater is equal to zero, so the balance of energy assumes the simple form – the work done by aerodynamic and friction forces is equal to the mechanical work in the joints.

In the planar model, the friction forces include a horizontal component of push-off force; hence in the planar model, the balance of energy consists of the work done by the push-off force Ry component (the work of the Rz component is equal to zero because of the constant distance between the ankle joint and the ice), joint moments and aerodynamic forces. The work of the Ry force component can reach a positive value of 100–200 J, so in the planar model there is no equivalence between the work of the joint moments and the work of the aerodynamic forces. The value of 'push-off work' is connected with the absence, in the 2-D model, of the sideward force Rx. The value of 'Ry work' is an approximate estimation of the work done to the sideward motion by moments in the skater's joints. The presence of mechanical work of push-off forces in the planar model's energy balance should not be considered as a reason to reject the planar simplification of the 3-D motion of the skater.

If it is assumed that the value of the mechanical work of the push-off forces in the planar model is equal to the sideward work of the skater, then equivalence between the work of the joint moments and aerodynamic forces should occur. Hence the difference between the work of the aerodynamic forces (W_A) and the sum of the positive and negative values of the work (W_P^m, W_N^m) of the joint moments indirectly estimates the accuracy of the planar simplification of skater motion relative to the forward motion of the skater in the 3-D model. For example, in variant 10 (Table 3), $W_A-(W_P^m-W_N^m)$ is equal to 35.7 J. If this value is divided by the total mechanical energy in the step (239 J), the estimation of planar simplification error is obtained, i.e. 14.9%. The total work in the joints is used as an estimation of the accuracy of the 2-D model, because this value is the criterion of technique effectiveness and it is not possible to determine where the planar model error is a positive or negative component of mechanical work.

In all variants investigated, the difference between the aerodynamic work and the total mechanical work in the joints lies between 6.8% (variant 1, Table 3) and 27.7% (variant 8, Table 3). A further way to check the accuracy of the planar simplification of 3-D motion is to investigate the zero-moment point (ZMP) trajectory on the push-off skate. The ZMP motion coincides with the length of the blade (see Fig. 15). The direction ZMP is from the heel to the toe of the blade, which corresponds to the physics of the push-off phase.

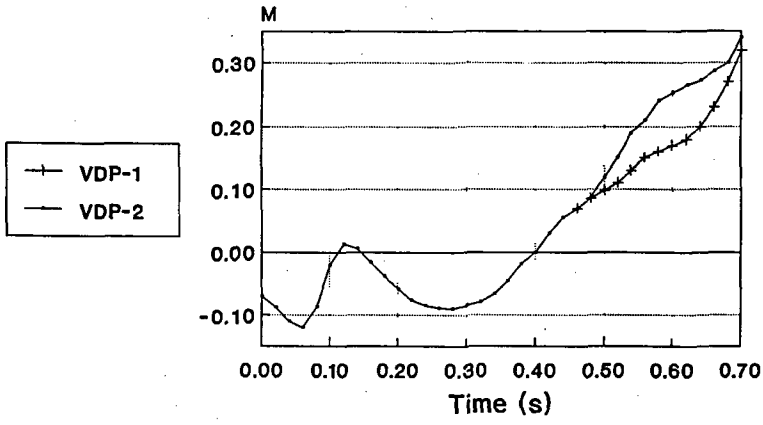

Figure 15 The trajectory of force point application (zero moment) when skating on the straight parts of the circuit. The displacement at the force point application on the support leg in phase 3 ($t>0.48$) is equal to 5 cm.